


## LTP Magnetic Field Interpolation

Doc. Ref.: **S2-IEC-OTH-3026**Issue: **1.0**Date: **25/Nov/2008**CI number: **L 3200**

### Approval List

	NAME	SIGNATURE	DATE
<b>Prepared by:</b>	M. Diaz-Aguiló E. García-Berro J.A. Lobo		25/Nov/2008
<b>Revised by:</b>			
<b>Approved by:</b>			
<b>Authorised by:</b>			

### Document Distribution List

Name	Position	Company
I. Lloro	Project Manager	IIEEC

	<b>DDS-LTP</b> LTP Magnetic Field Interpolation	<b>Ref.</b> S2-IEC-OTH-3026 <b>Version</b> 1.0 <b>Date</b> 25/Nov/2008 <b>Page</b> 3/26
--	--	--

### Document Status Sheet

Author	Issue	Date	Page(s)	Change description
First version	Version 1.0	25/Nov/2008	26	First version

## Table of Contents

Document Approval List . . . . .	1
Document Distribution List . . . . .	2
Document Status Sheet . . . . .	3
Table of Contents . . . . .	4
List of Figures . . . . .	5
List of Tables . . . . .	6
Acronyms . . . . .	6
Applicable documents . . . . .	6
Reference documents . . . . .	7
<b>1 Introduction</b>	<b>7</b>
<b>2 Theoretical approaches</b>	<b>7</b>
2.1 Multipole expansion . . . . .	8
2.2 Taylor expansion . . . . .	10
2.3 Distance weighting interpolation . . . . .	10
2.3.1 Balanced weighting interpolation . . . . .	11
2.3.2 Unbalanced weighting interpolation . . . . .	11
<b>3 Study objectives and overview</b>	<b>11</b>
<b>4 Simulating the magnetic field</b>	<b>12</b>
4.1 Calculation of the magnetic field inside the LCA . . . . .	12
4.2 The geometry of the magnetic field inside the LCA . . . . .	12
<b>5 Reconstruction of the magnetic field</b>	<b>15</b>
5.1 Multipole expansion . . . . .	17
5.2 Taylor expansion . . . . .	18
5.3 Distance weighting interpolation . . . . .	20
5.3.1 Balanced weighting interpolation . . . . .	20
5.3.2 Unbalanced weighting interpolation . . . . .	23
<b>6 Error analysis</b>	<b>23</b>
<b>7 Computing time</b>	<b>25</b>
<b>8 Conclusions</b>	<b>25</b>

## List of Figures

1.1	Qualitative behaviour of the magnetic field and gradient inside the LCA. Scales are not real. . . . .	8
4.1	Position of the test masses, the structure of the LCA, the 4 triaxial magnetometers and the 37 characterized magnetic dipolar sources (their size is proportional to their magnetic moment). . . . .	14
4.2	Contour plot of the average field within the LCA. The three field components $B_x$ , $B_y$ and $B_z$ and the modulus of the field are plotted showing the well of magnetic field inside the LCA. The positions of the magnetometers (black triangles) and of the test masses (red circles) are also represented. . . . .	15
4.3	Vectorial magnetic field at the test masses plane. . . . .	16
4.4	$x$ and $y$ components of the magnetic field, $\mathbf{B}$ , at the test masses plane. . . . .	16
4.5	Statistical distribution of the $xy$ position of the minimum of the field modulus inside the LCA volume. . . . .	17
5.1	Top panels: contour plot of the estimated field within the LCA volume for the case in which a multipole expansion is used. Bottom panels: errors in the estimates of the magnetic field within the LCA. The positions of the magnetometers (black triangles) and of the test masses (red circles) are also represented. . . . .	18
5.2	Top panels: contour plot of the estimated field within the LCA volume for the case in which a Taylor expansion is used. Bottom panels: errors in the estimates of the magnetic field within the LCA. The positions of the magnetometers (black triangles) and of the test masses (red circles) are also represented. . . . .	19
5.3	Errors in $B_x$ , $B_y$ , $B_z$ and $ \mathbf{B} $ as a function of the interpolation order. The top panel corresponds to test mass 1, while the bottom panel corresponds to test mass 2. . . . .	20
5.4	Top panels: contour plot of the estimated field within the LCA volume for the case in which a balanced weighting interpolation scheme used. In this figure $n = 1$ has been adopted. Bottom panels: errors in the estimates of the magnetic field within the LCA. The positions of the magnetometers (black triangles) and of the test masses (red circles) are also represented. . . . .	21
5.5	Top panels: contour plot of the estimated field within the LCA volume for the case in which a balanced distance weighting interpolation scheme used. In this figure $n = 0.5$ has been adopted. Bottom panels: errors in the estimates of the magnetic field within the LCA. The positions of the magnetometers (black triangles) and of the test masses (red circles) are also represented. . . . .	22
5.6	Top panels: contour plot of the estimated field within the LCA volume for the case in which a unbalanced distance weighting interpolation scheme is used. Bottom panels: errors in the estimates of the magnetic field within the LCA. The positions of the magnetometers (black triangles) and of the test masses (red circles) are also represented. . . . .	24

## List of Tables

3.1	Positions of the Test Masses . . . . .	11
3.2	Positions of the magnetometers . . . . .	12
3.3	S/C magnetic dipole sources and positions. . . . .	13
6.1	Errors of the magnetic field estimate at the positions of the test masses using different interpolation methods. . . . .	23
7.1	Computing time of the interpolation methods described here. See text for details. . . . .	25

## Acronyms

CI	Configuration Item
DDS	Data Management and Diagnostics Sub-System
IEEC	Institut d'Estudis Espacials de Catalunya
LTP	LISA Technology Package
LTPA	LTP Architect

## Applicable documents

Ref.	Title	Doc Number	Issue	Date
AD1	Magnetic Control on the LTP	LTP-Magnetics-TN-Iss001-Rev000	Issue 1	15/03/2004
AD2	Test report for LTP FM Magnetic Diagnostics	S2-IEC-TR-3067	Issue 1.1	22/10/2008
AD3	LTP EM TM Remnant Magnetic Moment Measurements	S2-EST-TR-3002	Issue 2	28/02/2007

 	<b>DDS-LTP</b>	<b>Ref.</b> S2-IEC-OTH-3026
	<b>LTP Magnetic Field Interpolation</b>	<b>Version</b> 1.0 <b>Date</b> 25/Nov/2008 <b>Page</b> 7/26

## Reference documents

Ref.	Title	Doc Number	Issue	Date
RD1	Science Requirements and Top-level Architecture Denition for the Lisa Technology Package (LTP)	LTPA-UTN-ScRD-Iss003-Rev1	Issue-3 Rev-3	30/06/2005

## 1 Introduction

Magnetic noise in the LTP can be a significant part of the total readout noise:  $1.2 \times 10^{-14} \text{ m s}^{-2} \text{ Hz}^{-1/2}$  out of  $3 \times 10^{-14} \text{ m s}^{-2} \text{ Hz}^{-1/2}$  is the allocated maximum acceleration magnetic noise budget out of the total system noise, in linear spectral densities<sup>1</sup>. This noise occurs because residual magnetisation and susceptibility in the proof masses couple to a surrounding magnetic field, giving rise to a force

$$\mathbf{F} = \left\langle \left[ \left( \mathbf{M} + \frac{\chi}{\mu_0} \mathbf{B} \right) \cdot \nabla \right] \mathbf{B} \right\rangle V \quad (1.1)$$

In this expression  $\mathbf{B}$  is the magnetic field in the test mass,  $\mathbf{M}$  stands for the density of the magnetic moment (namely, the magnetisation of the test mass),  $V$  is the volume of the test mass and  $\chi$  is its magnetic susceptibility. The rest of the symbols in this expression have their usual meaning. Finally the notation  $\langle \dots \rangle$  refers to the volume average of the enclosed quantity. Equation (1.1) shows that magnetic field and gradient fluctuations couple to DC values of the same magnitudes, due to the non-zero susceptibility of the test mass, to generate force — hence acceleration — noise.

It is important to realize that the sources of magnetic field are almost entirely due to various components inside the spacecraft (S/C), as the interplanetary magnetic field is orders of magnitude weaker. There is no source of magnetic field inside the LTP Core Assembly (LCA), all of them being placed within the S/C though outside the LCA walls.

In order to quantitatively assess the effect of magnetic noise, a set of magnetic sensors will be part of the LTP hardware. At some point, it was decided that four high sensitivity, tri-axial fluxgate magnetometers should be used to measure magnetic fields. The chosen fluxgate magnetometers carry relatively large sensing heads of high magnetic permeability, which are very easily magnetised and can therefore create unacceptably large back action fields. In order to reduce these fields, the magnetometers will be inserted in the LCA walls, somewhat far from the extrememly delicate and sensitive Inertial Sensor Heads (ISH). The counter-part of this strategy is that the actual value of the field in the test masses inferred from the readouts of the sensors will be more difficult to estimate.

This note is about how to implement in real practice the interpolation procedure to obtain magnetic field at the position of the test masses. As we shall see, the root of the problem can be traced to the space pattern of the magnetic field, which tends to decrease towards the inner parts of the LCA — of course due to the magnetic sources laying in the outer region of the LCA. Figure 1.1 provides a qualitative picture of the situation.

<sup>1</sup> See document LTPA-UTN-ScRD-Iss003-Rev1, *Science Requirements and Top-level Architecture Definition for the Lisa Technology Package (LTP) on Board LISA Pathfinder (SMART-2)*, Table 8.1.

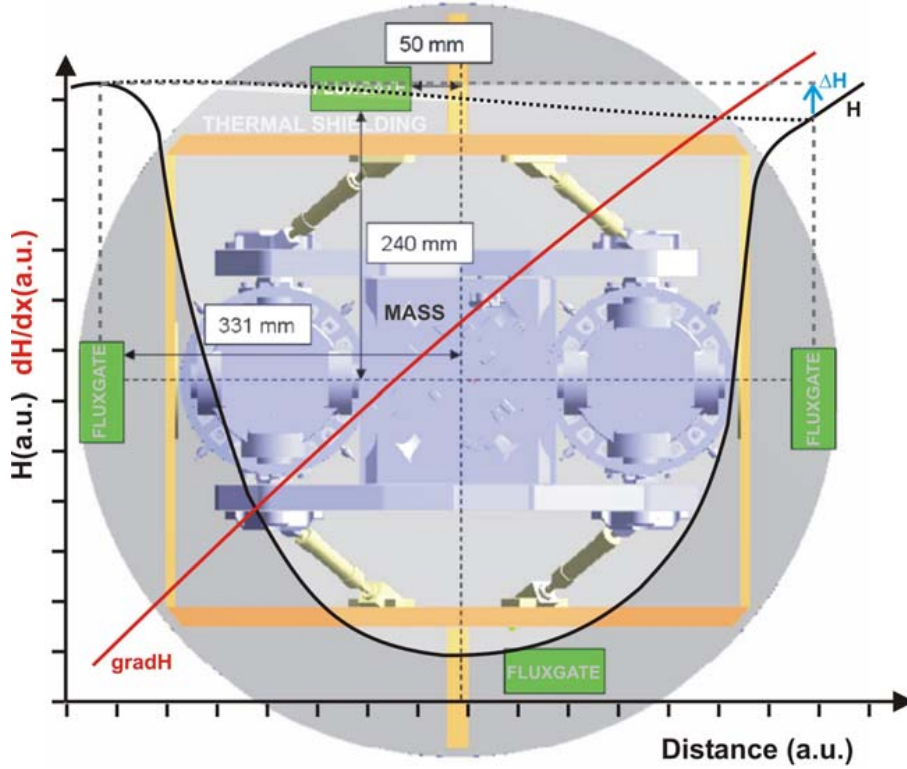


Figure 1.1: Qualitative behaviour of the magnetic field and gradient inside the LCA. Scales are not real.

## 2 Theoretical approaches

The objective is to reconstruct as accurately as possible the magnetic field inside the LCA on the basis of the information generated by the four readouts of the magnetometers. For this, the general theoretical framework will be briefly described.

### 2.1 Multipole expansion

We will treat the LCA region as a vacuum. This is a quite reasonably accurate hypothesis, as the materials inside it are essentially non-magnetic. Accordingly, the magnetic field has zero divergence and rotational<sup>1</sup>:

$$\nabla \cdot \mathbf{B}(\mathbf{x}, t) = 0 \quad \text{and} \quad \nabla \times \mathbf{B}(\mathbf{x}, t) = 0 \quad (2.1)$$

We thus have

$$\nabla \times \mathbf{B}(\mathbf{x}, t) = 0 \quad \Rightarrow \quad \mathbf{B}(\mathbf{x}, t) = \nabla \Psi(\mathbf{x}, t) \quad (2.2)$$

where  $\Psi(\mathbf{x}, t)$  is a scalar function. Because  $\nabla \cdot \mathbf{B}(\mathbf{x}, t) = 0$ , too, it immediately follows that  $\Psi(\mathbf{x}, t)$  is a harmonic function, or

$$\nabla^2 \Psi(\mathbf{x}, t) = 0 \quad (2.3)$$

<sup>1</sup>Given the distances in the spacecraft, of the order of one metre, propagation effects will be neglected. Time dependence will therefore be purely parametric, i.e., the time variable will just label the value the field has at that time.



	<b>DDS-LTP</b> <b>LTP Magnetic Field Interpolation</b>	<b>Ref.</b> S2-IEC-OTH-3026 <b>Version</b> 1.0 <b>Date</b> 25/Nov/2008 <b>Page</b> 9/26
--	---	--

The solution to this equation can be expressed as an orthogonal series of the form

$$\Psi(\mathbf{x}, t) = \sum_{l=0}^{\infty} \sum_{m=-l}^l M_{lm}(t) r^l Y_{lm}(\mathbf{n}) \quad (2.4)$$

where

$$r \equiv |\mathbf{x}|, \quad \mathbf{n} \equiv \mathbf{x}/r \quad (2.5)$$

are the spherical coordinates of the field point  $\mathbf{x}$ , whose origin is by (arbitrary) convention assumed in the geometric centre of the LCA. In equation (2.4), the terms in  $r^{-l-1}$  have been discarded, since the field cannot diverge at the centre of the LCA. Actually, the expansion given by Eq. (2.4) is only valid in a region interior to the closest field source. Finally, the coefficients  $M_{lm}(t)$ , which in the following will be called *multipole coefficients*, depend on the sources of magnetic field and on the boundary conditions.

To obtain the field components we substitute Eq. (2.4) into Eq. (2.2) obtaining:

$$\mathbf{B}(\mathbf{x}, t) = \nabla \Psi(\mathbf{x}, t) = \sum_{l=0}^{\infty} \sum_{m=-l}^l M_{lm}(t) \nabla [r^l Y_{lm}(\mathbf{n})] \quad (2.6)$$

In terms of the above development, the question we need to address is: how many terms of the series can we possibly determine on the basis of the available information? That is, how many terms of the series can be computed using the information provided by the magnetometers? Or, in other words, how many multipole coefficients can be calculated on the basis of the magnetometers readout data? Then, finally, to which accuracy can we estimate the actual magnetic field after the maximum number of multipole coefficients have been calculated?

The answer to the first two questions above is actually quite simple. The number of magnetometer data channels is 12, three channels per magnetometer, as the devices are in fact tri-axial. The approximate magnetic field is given by discarding terms in the series of Eq. (2.6) to include terms up to a maximum value of  $l = l_{\max} \equiv L$ , or

$$\mathbf{B}_{\text{estimated}}(\mathbf{x}, t) = \sum_{l=1}^L \sum_{m=-l}^l M_{lm}(t) \nabla [r^l Y_{lm}(\mathbf{n})] \quad (2.7)$$

The number of terms in this sum is

$$N(L) = \sum_{l=1}^L (2l + 1) = L(L + 2) \quad (2.8)$$

since the monopole ( $l = 0$ ) does not contribute. We thus have  $N(2) = 8$ , while  $N(3) = 15$ . This means that that we cannot pursue the series beyond the quadrupole ( $l = 2$ ) terms. Indeed, we only have 12 data channels, so we have some redundancy to determine  $M_{lm}(t)$  up to  $l = 2$ , but lack information to evaluate the next seven octupole terms<sup>2</sup>.

In order to make a best estimate of the coefficients  $M_{lm}(t)$ , a least square procedure is set up as follows. We define the quadratic error as

$$\varepsilon^2(M_{lm}) = \sum_{s=1}^4 |\mathbf{B}_{\text{measured}}(\mathbf{x}_s, t) - \mathbf{B}_{\text{estimated}}(\mathbf{x}_s, t)|^2 \quad (2.9)$$

<sup>2</sup> A clarification is in order here. The multipole coefficients  $M_{lm}(t)$  are actually *complex* numbers, which may mislead one into inferring that *fewer* can actually be calculated. This is however not so because of the symmetry  $M_{lm}(t) = (-1)^m M_{l,-m}^*(t)$ , which ensures that  $\mathbf{B}(\mathbf{x}, t)$  is a real number.

	<b>DDS-LTP</b> <b>LTP Magnetic Field Interpolation</b>	<b>Ref.</b> S2-IEC-OTH-3026 <b>Version</b> 1.0 <b>Date</b> 25/Nov/2008 <b>Page</b> 10/26
--	---	---

where the sum extends over the number of magnetometers, situated at positions  $\mathbf{x}_s$  ( $s = 1, \dots, 4$ ), and then find those values of  $M_{lm}$  which minimise that error:

$$\frac{\partial \varepsilon^2}{\partial M_{lm}} = 0 \quad (2.10)$$

Once this system of equations is solved, the estimated coefficients  $M_{lm}$  are replaced into Eq. (2.7), then the spatial arguments are substituted by the positions of the test masses to finally obtain the sought extrapolations. This process needs to be repeated for each instant  $t$  at which measurements are taken, thereby generating the magnetic field time series. The gradient is also recovered by taking the derivative of Eq. (2.7):

$$\frac{\partial B_i}{\partial x_j}(\mathbf{x}, t) = \sum_{lm} M_{lm}(t) \frac{\partial^2}{\partial x_i \partial x_j} [r^l Y_{lm}(\mathbf{n})] \quad (2.11)$$

## 2.2 Taylor expansion

A different way of performing the estimation of the magnetic field is provided by a Taylor expansion of the magnetic field in a Taylor series around the positions of the test masses. As shown in the previous section, only up to quadrupole terms can be determined with the information supplied by 12 magnetometer data channels. We thus demonstrated that the multipole series has to be truncated when only *linear* terms in the coordinates are included<sup>3</sup>. The estimated field can therefore be also represented by

$$B_{\text{estimated}, i}(\mathbf{x}, t) = \alpha_i(t) + \sum_{j=1}^3 \beta_{ij}(t) [x_j - x_{\text{TM}, j}] \quad (2.12)$$

where  $\mathbf{x}_{\text{TM}}$  is the position of a particular test mass, and

$$\alpha_i(t) = B_{\text{estimated}, i}(\mathbf{x}_{\text{TM}}, t) \quad \text{and} \quad \beta_{ij}(t) = \partial_j B_{\text{estimated}, i}(\mathbf{x}_{\text{TM}}, t) \quad (2.13)$$

with the additional properties

$$\beta_{ij}(t) = \beta_{ji}(t) \quad \text{and} \quad \sum_{i=1}^3 \beta_{ii}(t) = 0 \quad (2.14)$$

The idea is now to determine  $\alpha_i$  and  $\beta_{ij}$ , a total 8 independent unknowns, by the least square method of Eqs. (2.9) and (2.10). The method is of course identical to the multipole expansion, but has some computational advantages in that it directly yields the magnetic field and gradient in the test masses, and does not require complex number algebra.

## 2.3 Distance weighting interpolation

We have already shown that there are physical methods to interpolate the value of the magnetic field inside the LCA. Yet there is another purely empirical method for estimating  $\mathbf{B}$  at the positions of the test masses. We discuss two different approaches in the next subsections.

<sup>3</sup> This derives from the fact that  $r^l Y_{lm}(\mathbf{n})$  is a polynomial of degree  $l$  in  $(x, y, z)$ , so that  $\nabla[r^l Y_{lm}(\mathbf{n})]$  are polynomials of degree  $l - 1$ .

	<b>DDS-LTP</b>	<b>Ref.</b>	S2-IEC-OTH-3026
	LTP Magnetic Field Interpolation	<b>Version</b>	1.0
		<b>Date</b>	25/Nov/2008
		<b>Page</b>	11/26

### 2.3.1 Balanced weighting interpolation

This first method used to estimate the field within the interior of the LCA consists in computing the field as a weighted sum of the different measures of the 4 triaxial magnetometers. This calculation will be performed as follows:

$$\mathbf{B}_{\text{estimated}} = \sum_{i=1}^4 a_i \mathbf{B}_i \quad (2.15)$$

where  $\mathbf{B}_i$  are the readouts of the magnetometers, and weighting factors  $a_i$  are inversely proportional (to the  $n$  power) to the distance between the point at which the field must be estimated and the specified magnetometer:

$$a_i = \frac{1/r_i^n}{\sum_{j=1}^4 1/r_j^n} \quad (2.16)$$

In this expression  $n$  specifies the order of the interpolation. The determination of the order of this specific interpolation may be performed by an statistical analysis over the different field distributions and values of  $n$ . This procedure will ensure a good average interpolation scheme, but it will not ensure an optimal performance for an specific set of directions for the magnetic dipole sources.

### 2.3.2 Unbalanced weighting interpolation

In this case we use again Eq. (2.16), but in this case we allow the value of  $n$  to be different for each one of the components of the magnetic field. We are aware that this is not a self-consistent way of interpolating the magnetic field, but we want to check whether or not allowing for more degrees of freedom we obtain a better estimate of each individual component of the magnetic field.

## 3 Study objectives and overview

The reminder of this note is to assess the performance of the different interpolation methods described above under realistic circumstances. A consolidated datum is the positions of the test masses and magnetometers. These are referred to a coordinate system rigidly associated to the spacecraft structure. In that system, they are given in tables 3.1 and 3.2<sup>1</sup>. The positions of the test masses and the magnetometers are specified in table 3.1 and table 3.2 respectively.

Table 3.1: Positions of the Test Masses

Test mass	$x$ [m]	$y$ [m]	$z$ [m]
1	-0.1880	0	0.4784
2	0.1880	0	0.4784

As can be seen on inspection of these tables, the magnetometers are quite far from the test masses, which characterises the field interpolation problem as a very challenging objective.

The methodology we will use is the following one. We model the magnetic field in the spacecraft as one generated by a set of point magnetic dipoles, whose DC magnetic moments and positions are fixed and whose directions are random. We then statistically analyse the results after a large number of runs

<sup>1</sup>Thanks are due to Dave Wealthy, from ASU, who kindly supplied them in November 2006.

Table 3.2: Positions of the magnetometers

Magnetometer	$x$ [m]	$y$ [m]	$z$ [m]
1	-0.0758	0.3694	0.4784
2	-0.3765	0	0.4784
3	0.0758	-0.3694	0.4784
4	0.3765	0	0.4784

in which the dipole directions are randomly set. A precise knowledge of the magnetic field sources is not available at the time of writing this technical note. In fact, there are a number of identified sources in the spacecraft which still lack full magnetic characterisation. When the flight model parts will be ready, they will be magnetically characterised as point dipoles. This is due to major experimental difficulties in obtaining more detailed information, and can be accepted given their relatively large distance to the test masses. An exception to this is the solar panel structure, which will not be considered here. Rough preliminary estimates of the magnetic moments of the identified parts have been made by ASU, the result being just the modulus of the dipoles of those parts. The latter are at least 37, and the data are shown in table 3.3. We feel that the simulations based on these data do provide a good approximation of the interpolation performance, and we therefore consider they are realistic.

## 4 Simulating the magnetic field

### 4.1 Calculation of the magnetic field inside the LCA

The calculation of any magnetic field once all dipolar sources creating this field are perfectly known and determined is rather straightforward. In this particular case, taking into account the current status of LTP, only their positions and their dipolar momentum have been determined (the exact direction of this momentum have not yet been specified). Thus, the magnetic field inside the LCA may be analysed only with a set of sources with random directions. Consequently, this will highly affect to the randomness of the field reconstructed, which will be different for each realization. This lack of knowledge about the exact behavior of the field inside LCA makes even more difficult its estimation. In any case, foreseeing that these directions would be determined in a subsequent phase of the implementation of the spacecraft, a first analysis may be performed taking into account an statistical analysis of these directions. Until now, the only known configuration is the exact position of the 4 triaxial magnetometers, those of the 2 test masses and the exact position and dipolar momentum of the 37 characterized magnetic sources — see figure 4.1. This information will be used in the next sections in order to reconstruct the real field and implement the different interpolation methods.

### 4.2 The geometry of the magnetic field inside the LCA

The magnetic field produced by each of the dipoles in table 3.3 is given by

$$\mathbf{B}_i(\mathbf{r}_i) = \frac{\mu_0}{4\pi} \frac{3(\mathbf{m}_i \cdot \hat{\mathbf{r}}_i)\hat{\mathbf{r}}_i - \mathbf{m}_i}{|\mathbf{r}_i|^3} \quad (4.1)$$

where  $\mathbf{r}$  is the relative vector from each dipolar source to each field point and  $\mathbf{m}$  is the dipolar

Table 3.3: S/C magnetic dipole sources and positions.

$ \mathbf{m} $ [mA m <sup>2</sup> ]	$x$ [m]	$y$ [m]	$z$ [m]
50.0	0.2097	0.6395	0.4759
100.0	0.2435	-0.6554	0.5380
100.0	0.3520	-0.5020	0.5999
150.0	0.4770	0.6986	0.4500
150.0	0.3355	0.4528	0.6000
75.0	0.4455	0.7348	0.7274
25.0	-0.3414	-0.7602	0.2460
25.0	0.4980	-0.9909	0.4755
25.0	-0.6000	0.9353	0.4400
50.0	-0.7855	-0.6189	0.9850
50.0	-0.6744	-0.7121	0.9850
50.0	-0.5634	-0.8053	0.9850
25.0	-0.5555	0.0340	0.4659
25.0	0.5555	-0.0340	0.4659
50.0	-0.4319	0.5769	-0.0020
50.0	0.4319	0.5769	-0.0020
50.0	-0.5774	0.2245	0.2900
50.0	-0.5774	0.2245	0.6500
100.0	0.0000	-0.9601	0.4784
100.0	0.8315	0.4800	0.4784
100.0	-0.8315	0.4800	0.4784
300.0	-0.0308	-0.7858	0.3000
300.0	0.6008	0.5424	0.3620
300.0	-0.6698	0.4181	0.3000
300.0	-0.2626	-0.8355	0.6382
30.0	-0.6000	-0.2721	0.5945
30.0	-0.2404	-0.6005	0.6300
30.0	-0.2370	0.6211	0.4800
30.0	-0.4197	0.5176	0.5800
30.0	-0.3694	-0.5559	0.3220
10.0	-0.4276	0.5576	0.2850
100.0	-0.4137	-0.5353	0.6000
10.0	0.4481	-0.5264	0.2740
25.0	0.5641	-0.7178	0.5954
20.0	0.5800	-0.7179	0.2920
30.0	0.5850	-0.2760	0.6000
10.0	-0.6240	-0.1675	0.4500

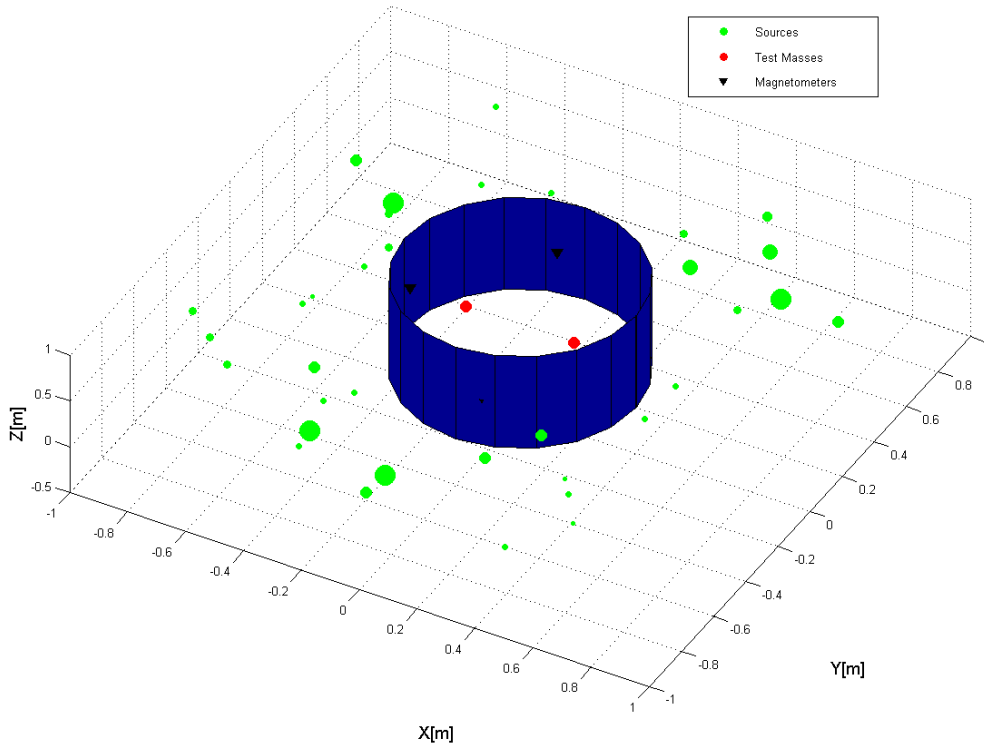


Figure 4.1: Position of the test masses, the structure of the LCA, the 4 triaxial magnetometers and the 37 characterized magnetic dipolar sources (their size is proportional to their magnetic moment).

momentum of each source. The total field is obtained by adding the fields generated by each of the magnetic sources. Since we do not know the precise direction of the magnetic moment of each dipolar source we have simulated  $10^3$  magnetic field configurations with random directions of the dipoles and we have averaged them. The average magnetic field obtained within the LCA is represented in figure 4.2. This magnetic field is compliant with DC Magnetic field requirement (smaller than  $10\mu\text{m}$ ).

As it may be observed, the fact of estimating the field at the positions of the test masses may be difficult with only 4 magnetometers due to the vectorial nature of the magnetic field. In order to further analyze this in figure 4.3 we show the vectorial characteristic of the average magnetic field whereas in figure 4.4 we show the average  $B_x$  and  $B_y$  components on the plane of the test masses. As can be seen the magnetic field has a saddle point midway the test masses and, moreover, the magnetic field is rather steep as we move away of this point, presenting large variations. This is due to the superposition of many different dipolar sources. Thus, estimating the field at the positions of the test masses would only be possible if the gradients of the magnetic field are accurately determined.

We stress that in figures 4.3 and 4.4 we display the *average* magnetic field. However, the position of the saddle point strongly depends on the particular configuration of the magnetic dipoles of the sources, which we remind are chosen randomly. To illustrate the large degree of variation of the position of the minimum of the magnetic field in figure 4.5 we display an histogram showing the distribution of the positions of the minimum of the magnetic field obtained after  $10^3$  realizations. As it can be observed, the minimum of the magnetic field is always placed within the LCA geometry, but there is no preferred position. This figure illustrates the large dependence of the position of the saddle point on the specific

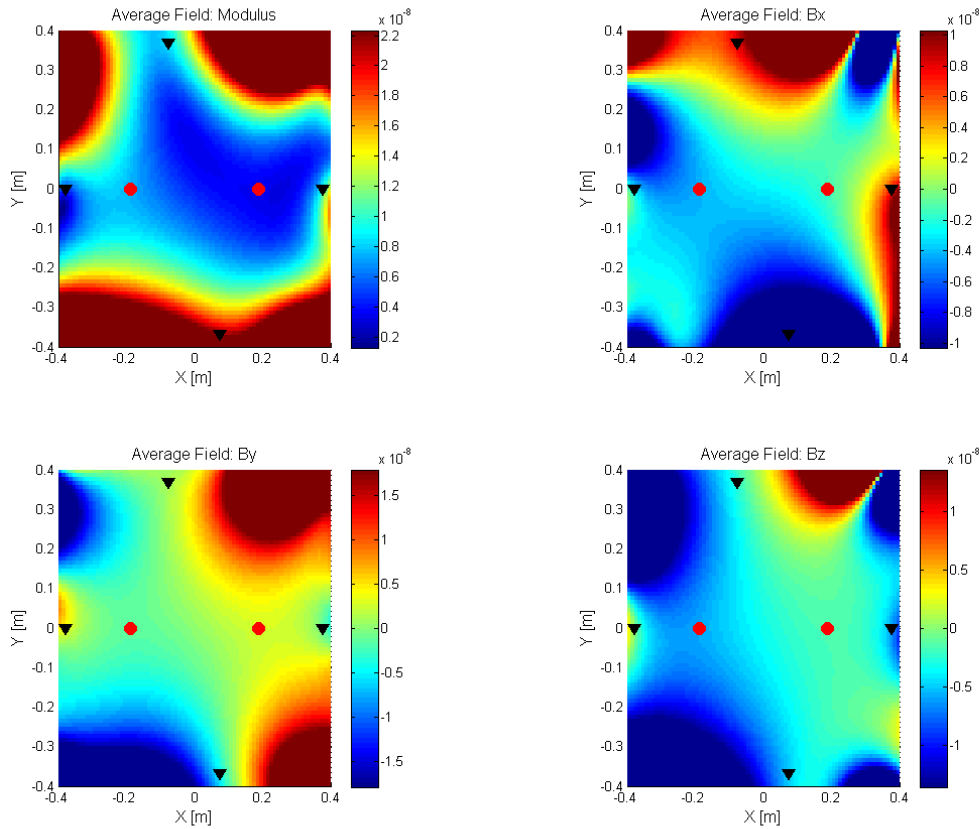


Figure 4.2: Contour plot of the average field within the LCA. The three field components  $B_x$ ,  $B_y$  and  $B_z$  and the modulus of the field are plotted showing the well of magnetic field inside the LCA. The positions of the magnetometers (black triangles) and of the test masses (red circles) are also represented.

directions of the dipolar moments of the magnetic sources.

## 5 Reconstruction of the magnetic field

One of the goals of the Data Diagnostics Subsystem is to estimate the environmental conditions inside the LCA, and particularly the magnetic conditions. Specifically, using the readouts of the magnetometers we should be able to estimate the value of the magnetic field and of its gradient at the positions of the test masses. This, in turn, would allow to estimate acceleration noise due to the force generated by the magnetic field on each of the test masses. The ability of doing a good estimation of this quantity will yield one step forward in the objective of discriminating all noise sources. For this purpose in this section we test the different approaches detailed in section 2.

In order to better understand the results obtained using each of the methods previously described an error analysis should be performed for each of the components of the magnetic field. In this docu-

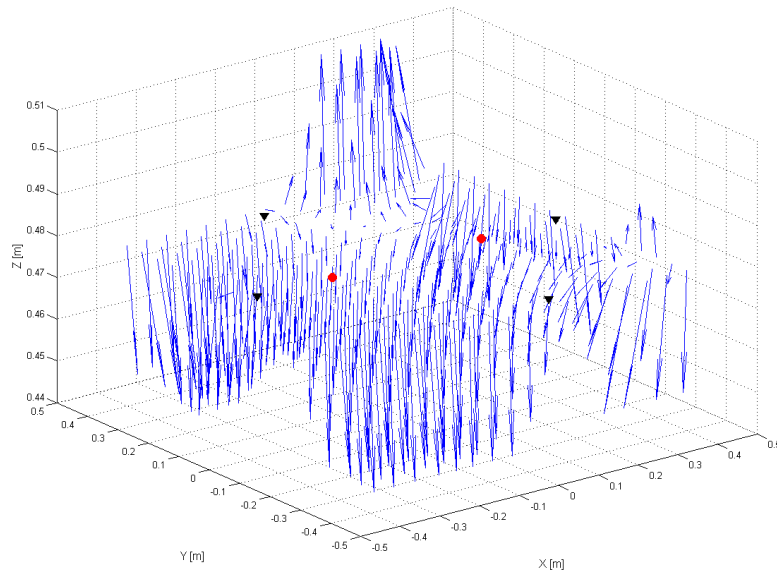


Figure 4.3: Vectorial magnetic field at the test masses plane.

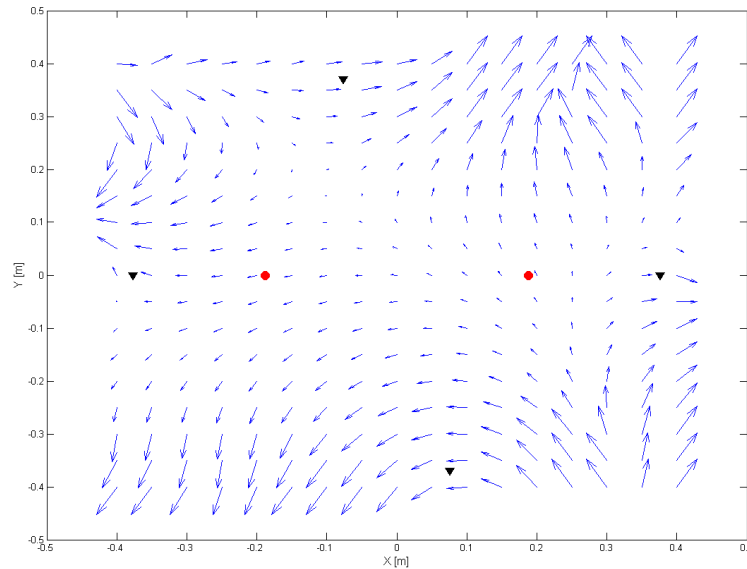


Figure 4.4:  $x$  and  $y$  components of the magnetic field,  $\mathbf{B}$ , at the test masses plane.

ment two different errors have been computed. The first and most straightforward way of computing errors is to compare the value of each of the components of the reconstructed magnetic field with the corresponding component of the input magnetic field. For instance, in the case of the  $x$  component of the magnetic field, we have:



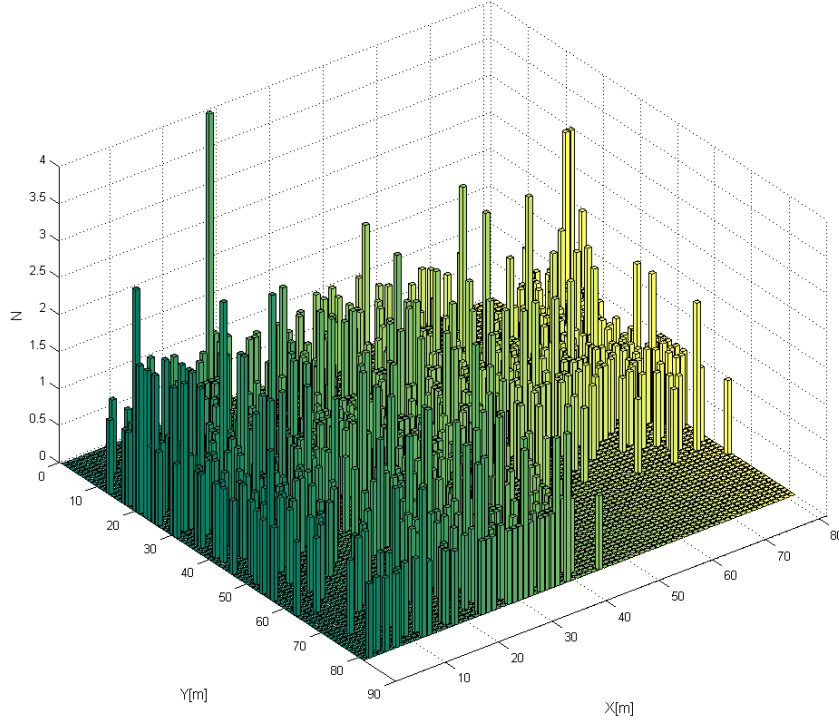


Figure 4.5: Statistical distribution of the  $xy$  position of the minimum of the field modulus inside the LCA volume.

$$\varepsilon_x^1 = \frac{B_{\text{estimated}_x} - B_{\text{real}_x}}{B_{\text{real}_x}} \quad (5.1)$$

This is done for each of the components of the magnetic field. However, a close inspection of figures 4.3 and 4.4 reveals that some of the components of the magnetic field are very close to zero at the positions of the test masses. Consequently, we also implement an alternative way of computing the error, taking into account that the modulus of the magnetic field is never zero:

$$\varepsilon_x^2 = \frac{B_{\text{estimated}_x} - B_{\text{real}_x}}{|\mathbf{B}_{\text{real}}|} \quad (5.2)$$

The first expression probably leads to an overestimate of the error while the second one most likely underestimates the error. In all the cases tested below we always average the errors of each component of the magnetic field over  $10^3$  realizations.

## 5.1 Multipole expansion

A multipole expansion provides a first order approximation to the magnetic field. Thus we expect a constant gradient in each one of the directions inside the LCA volume. The four top panels of figure 5.1 show that this is indeed the case. Thus, using this approximation does not allow to reproduce the magnetic well inside the LCA. However, it performs an acceptable estimation of the field at the test masses positions, as shown in the four bottom panels of figure 5.1.

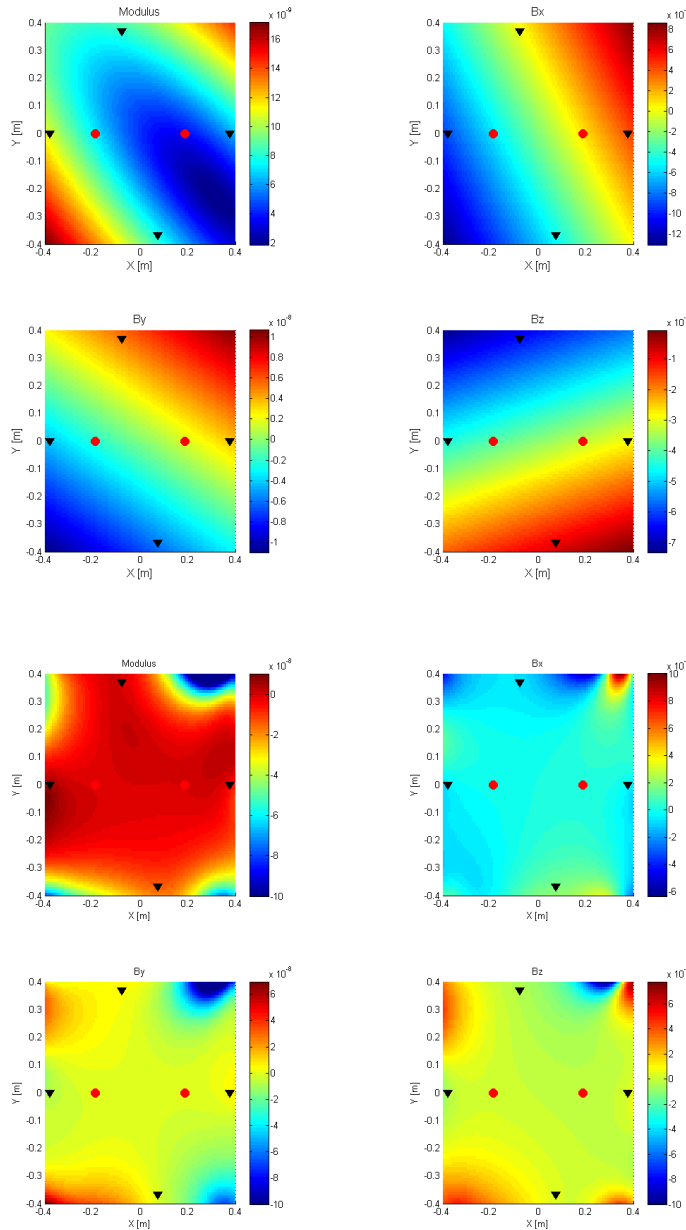


Figure 5.1: Top panels: contour plot of the estimated field within the LCA volume for the case in which a multipole expansion is used. Bottom panels: errors in the estimates of the magnetic field within the LCA. The positions of the magnetometers (black triangles) and of the test masses (red circles) are also represented.

## 5.2 Taylor expansion

As previously mentioned the results obtained using a Taylor expansion are also a first order approximation to the magnetic field. Thus, we expect that these results should be identical to those obtained using a multipole expansion. Consequently, we expect also in this case a constant gradient in each one of the directions inside the LCA volume. This is borne out by examining the four top panels of

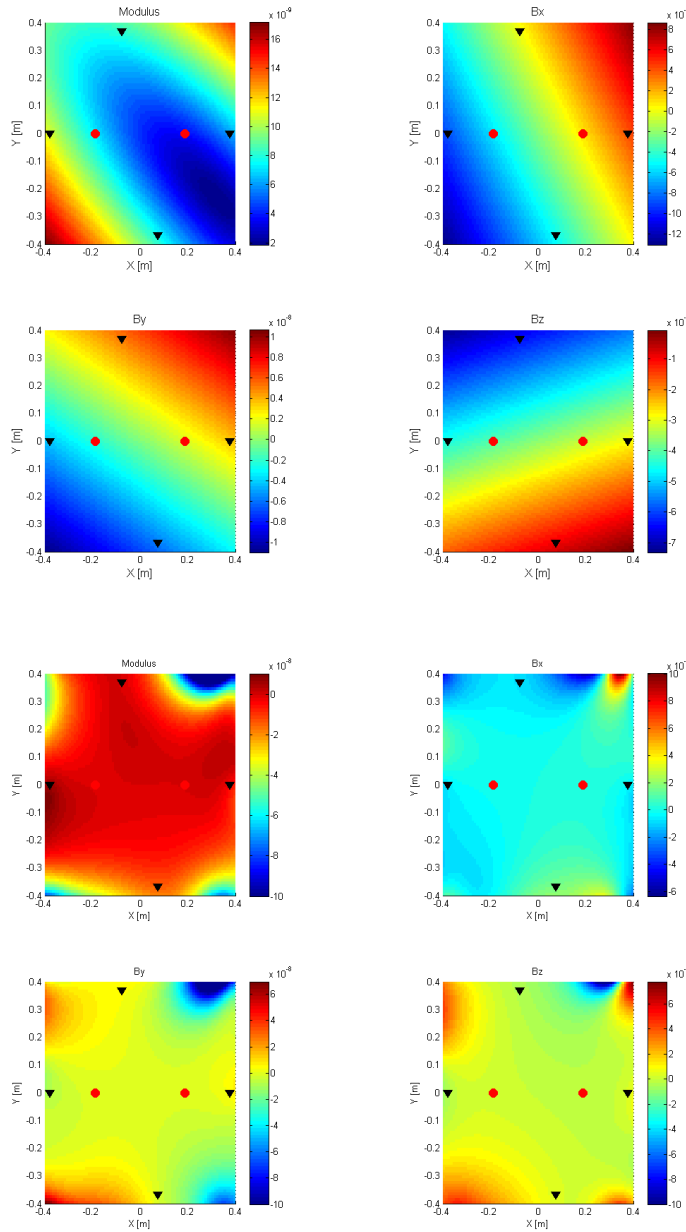


Figure 5.2: Top panels: contour plot of the estimated field within the LCA volume for the case in which a Taylor expansion is used. Bottom panels: errors in the estimates of the magnetic field within the LCA. The positions of the magnetometers (black triangles) and of the test masses (red circles) are also represented.

figure 5.2, which must be compared with those of figure 5.1. Indeed, we find that the magnetic configuration is the same obtained previously. Thus, again we reach the same conclusions, namely, that this approximation does not reproduce the magnetic well inside the LCA, but an acceptable estimation of the field at the test masses positions is obtained.

### 5.3 Distance weighting interpolation

#### 5.3.1 Balanced weighting interpolation

The determination of the most appropriate order of interpolation,  $n$ , for this specific interpolation scheme is done by performing a statistical analysis over different magnetic field configurations and values of  $n$ . Accordingly, we have studied the errors in the reconstructed magnetic field taking into account  $10^3$  magnetic configurations and values of  $n$  ranging between 0 and 2. However, it should be taken into account that the value of  $n$  which minimizes the interpolation error will ensure a good average interpolation scheme, but it will not ensure an optimal performance for a specific set of directions of the magnetic dipolar sources. The results are shown in figure 5.3. The top panel corresponds to the results obtained for test mass 1, while the bottom panel corresponds to the results obtained for test mass 2. The errors have been computed according to Eq. (5.1).

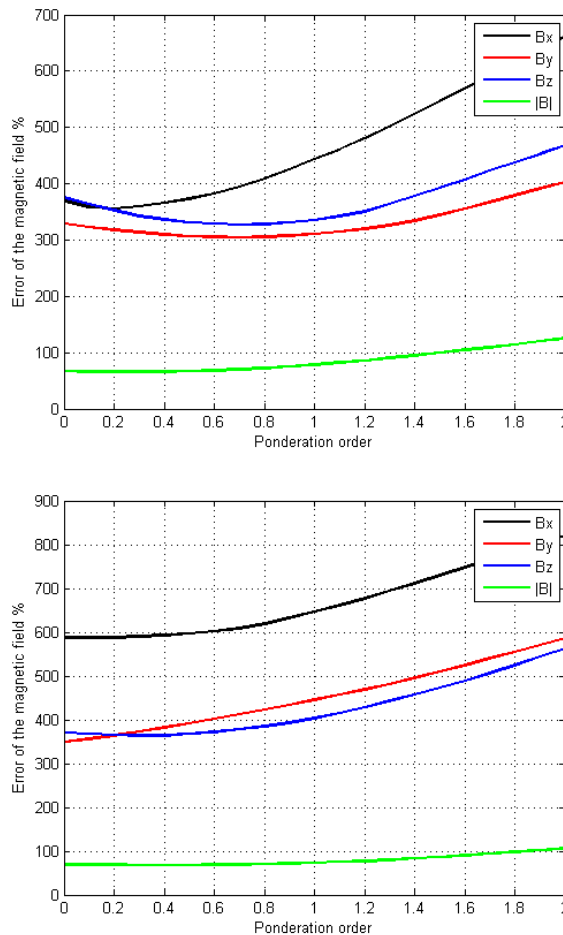


Figure 5.3: Errors in  $B_x$ ,  $B_y$ ,  $B_z$  and  $|\mathbf{B}|$  as a function of the interpolation order. The top panel corresponds to test mass 1, while the bottom panel corresponds to test mass 2.

It is worth mentioning that the minimum error for the modulus of the magnetic field occurs at different values of  $n$  for each test mass. The same holds for each of the components of the magnetic field. Specifically, while for test mass 1 there are clear minima around  $n = 0.5$  this is not the case for test mass 2, where the relative error increases for increasing values of  $n$ . Moreover, the values of  $n$  which give a minimum in the components of the magnetic field at the position of test mass 1 are not

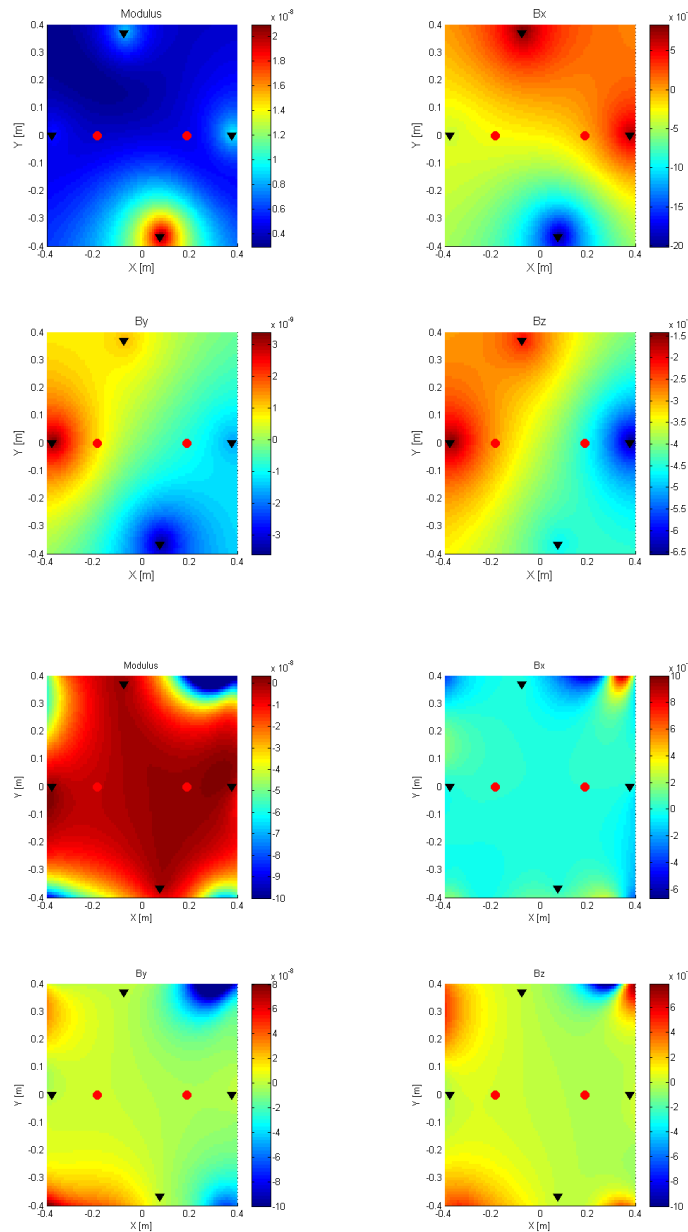


Figure 5.4: Top panels: contour plot of the estimated field within the LCA volume for the case in which a balanced weighting interpolation scheme used. In this figure  $n = 1$  has been adopted. Bottom panels: errors in the estimates of the magnetic field within the LCA. The positions of the magnetometers (black triangles) and of the test masses (red circles) are also represented.

coincidental for all three components.

The reconstructed magnetic field is shown in figures 5.4, in which we have adopted  $n = 1$  for all field components, and 5.5, for which  $n = 0.5$  was used. The bottom panels of these figures show, respectively, the interpolating errors. As can be seen in these figures the geometry of the average field is reproduced fairly well — compare with figure 4.2 — but, nevertheless, the errors continue to

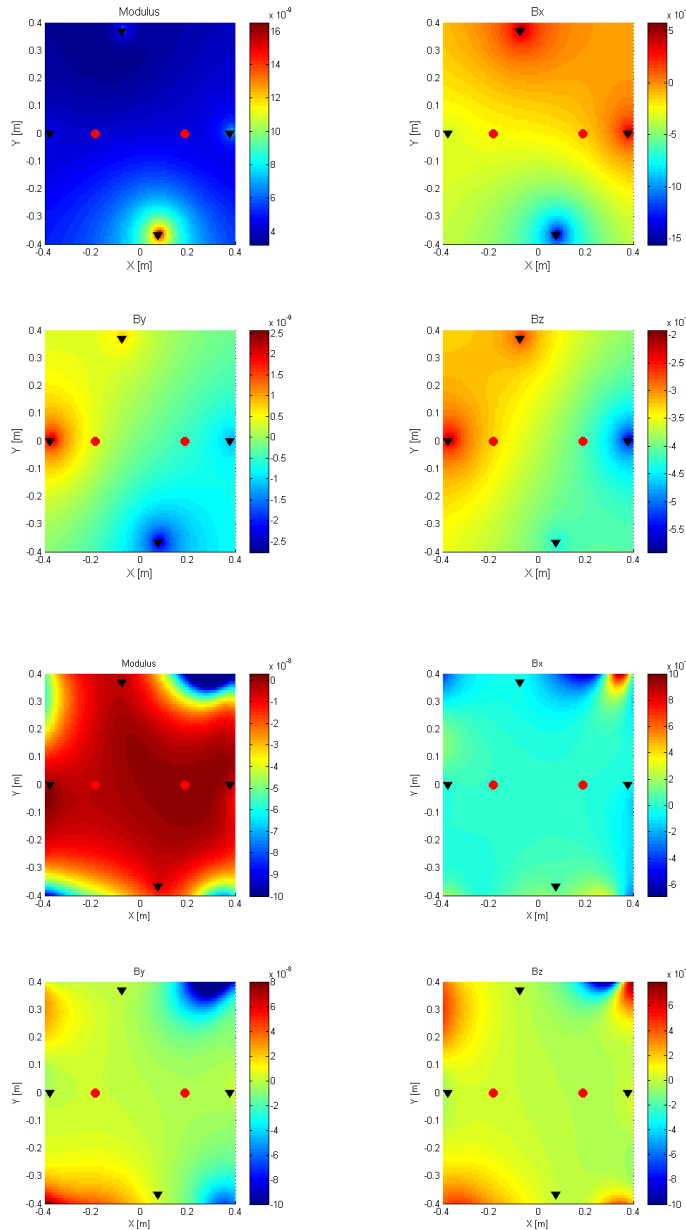


Figure 5.5: Top panels: contour plot of the estimated field within the LCA volume for the case in which a balanced distance weighting interpolation scheme used. In this figure  $n = 0.5$  has been adopted. Bottom panels: errors in the estimates of the magnetic field within the LCA. The positions of the magnetometers (black triangles) and of the test masses (red circles) are also represented.

be unacceptable in both cases. Moreover, as clearly depicted in these figures when this interpolating method is used we do not obtain constant gradients inside the volume of the LCA, as it was the case with the multipole and Taylor expansions. In fact, the field inside the LCA is reconstructed with similar distributions to the real one but, obviously, not exactly. Again, the limitation of having only 4 magnetometers and quite far from the interpolation point makes difficult the reconstruction of the

magnetic field.

### 5.3.2 Unbalanced weighting interpolation

In this case, as explained in section 2.3.2, we use different values of  $n$  for each field component. Actually this method presents some difficulties because in order to compute the optimal values of  $n$  for each field component the real field value is needed, which is obviously not available. Additionally, the values of  $n$  which are optimal for each of the components of the magnetic field are different for each position inside the LCA. This is borne out from an inspection of figure 5.3. Clearly the values of  $n$  which are optimal are different for each one of the test masses and components of the magnetic field. Hence, we have chosen to adopt the values which are optimal for the center of the interferometer. These values of  $n$  are  $n = 0.1$  for  $B_x$ ,  $n = 2$  for  $B_y$  and  $n = 0.1$  for  $B_z$ . The resulting reconstructed magnetic field is shown in figure 5.6. Clearly we do not obtain significantly better results.

## 6 Error analysis

Table 6.1: Errors of the magnetic field estimate at the positions of the test masses using different interpolation methods.

Error (%)	$B_x$	$B_y$	$B_z$	$ \mathbf{B} $
Multipole Expansion				
$\varepsilon_{TM_1}^1$	493.7	330.5	359.5	88.6
$\varepsilon_{TM_1}^2$	87.4	55.5	51.6	88.6
$\varepsilon_{TM_2}^1$	640.4	543.1	368.2	75.7
$\varepsilon_{TM_2}^2$	84.8	59.6	43.8	75.7
Taylor Expansion				
$\varepsilon_{TM_1}^1$	493.7	330.5	359.5	88.6
$\varepsilon_{TM_1}^2$	87.4	55.5	51.6	88.6
$\varepsilon_{TM_2}^1$	640.4	543.1	368.2	75.7
$\varepsilon_{TM_2}^2$	84.8	59.6	43.8	75.7
Balanced $n = 1$				
$\varepsilon_{TM_1}^1$	441.4	328.9	343.0	78.3
$\varepsilon_{TM_1}^2$	80.9	54.1	46.2	78.3
$\varepsilon_{TM_2}^1$	612.6	462.0	391.3	71.6
$\varepsilon_{TM_2}^2$	83.4	59.4	41.9	71.6
Balanced $n = 1/2$				
$\varepsilon_{TM_1}^1$	375.3	334.2	339.9	67.2
$\varepsilon_{TM_1}^2$	71.1	53.7	44.2	67.2
$\varepsilon_{TM_2}^1$	555.5	412.7	356.6	66.9
$\varepsilon_{TM_2}^2$	78.9	61.5	40.4	66.9
Unbalanced $n$				
$\varepsilon_{TM_1}^1$	468.8	495.5	1380.4	190.0
$\varepsilon_{TM_1}^2$	77.4	140.7	93.5	189.9
$\varepsilon_{TM_2}^1$	649.4	806.8	1081.6	220.4
$\varepsilon_{TM_2}^2$	89.4	165.2	109.0	220.4

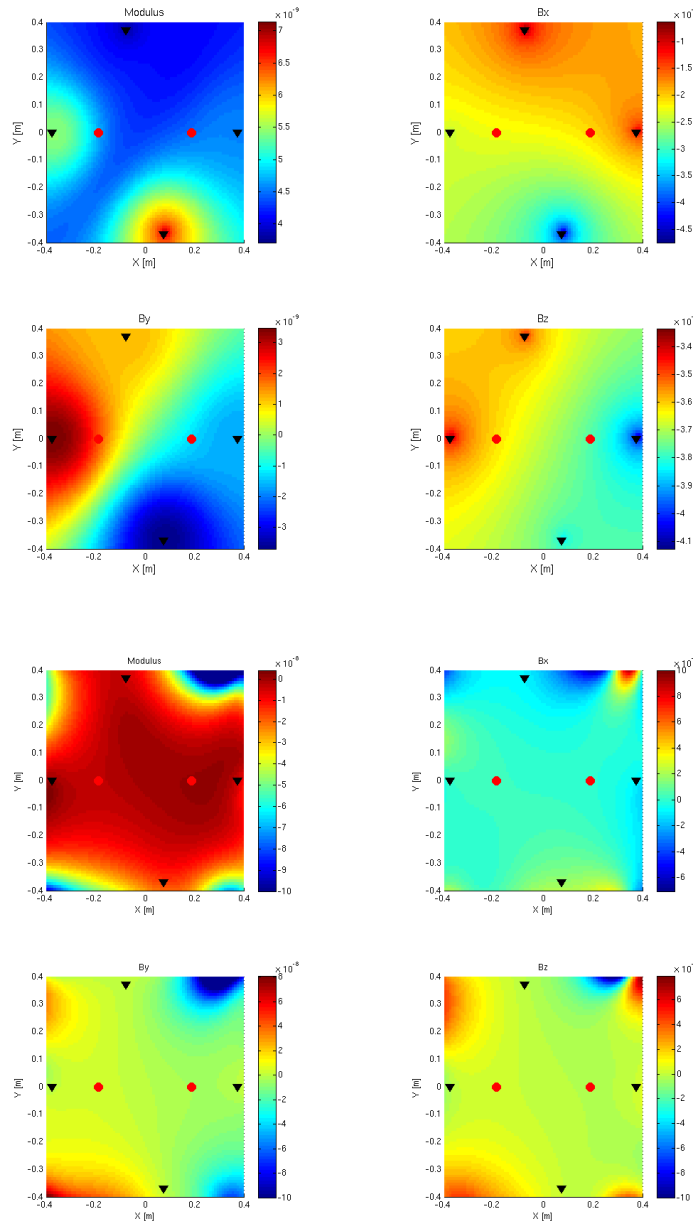


Figure 5.6: Top panels: contour plot of the estimated field within the LCA volume for the case in which a unbalanced distance weighting interpolation scheme is used. Bottom panels: errors in the estimates of the magnetic field within the LCA. The positions of the magnetometers (black triangles) and of the test masses (red circles) are also represented.

This table shows that the unbalanced weighting interpolation method does not perform correctly. This is due to the fact that every magnetic field realization is highly uncorrelated, and the fact of choosing the best orders for a set of directions (even if an average is performed) it does not assure a good performance for a different field realization.

On the other hand, it also proves that the balanced weighting interpolation method with a fixed value of  $n = 0.5$  can achieve mean errors around 300% in nearly all the field components. These errors



are  $\sim 60\%$  when Eq. (5.2) is used. At the same time, a Taylor expansion seem to be less stable than the distance interpolation method due to the fact of estimating a constant gradient. This aspect does not permit the algorithm to neglect a measurement that might be misleading due to a peak of field in the boundaries of the magnetometer.

Therefore, after this analysis, even though no method offers an acceptable estimation, it may be concluded that currently the only algorithms capable of presenting stable and acceptable errors are the distance weighting method with  $n = 0.5$  and the Taylor expansion.

## 7 Computing time

Another interesting aspect to be taken into account in the present analysis is an evaluation of the computing time consumed by each interpolation method. This comparison may lead to a trade-off between quality of the estimated magnetic field and consumed computing time. For the different algorithms, the computing times are specified in table 7.1.

Table 7.1: Computing time of the interpolation methods described here. See text for details.

Method	Computing time [s]
Distance weighting	$4.7 \times 10^{-4}$
Multipole expansion	0.4553
Taylor expansion	0.0792

As clearly observed in this table, the fastest method is the weighting interpolation method, because no iterations are required for obtaining the estimated field. On the other hand, a comparison between the multipole expansion and the Taylor expansion reveals that their computing times differ by an order of magnitude. This is due to the usage of the complex variables in the case of the multipole expansion. Additionally, the estimated magnetic field obtained using the distance weighting method also presents a better error stability. All in all this last method offers the best performances for estimating the magnetic field inside the LCA.

## 8 Conclusions

The objective of estimating the exact magnetic field within the LCA volume using fast interpolation methods with an acceptable accuracy is highly restricted by two reasons. The first one is that to proceed with this estimation, only 4 measures are available, because the diagnostics subsystems has been set only with 4 triaxial magnetometers, thus restricting very much the amount of information available. The second reason is that the location of the magnetometers is not convenient. In fact, the magnetomers are placed more than 20 cm away from the positions of the test masses. This is a considerable distance in order to perform a good quality estimation of a vectorial field inside the LTP configuration. These two aspects are a clear limiting factor to any interpolation method. The fact of having only 4 magnetometers only allows to perform first order approximations. Obviously these kind of approximations are very limiting if the objective is representing a vectorial field that has a well within the LCA volume and each of its components has a saddle point. Nevertheless we have tested the accuracy of several interpolation methods. In particular, we have implemented a

 	<b>DDS-LTP</b>  <b>LTP Magnetic Field Interpolation</b>	<b>Ref.</b> S2-IEC-OTH-3026 <b>Version</b> 1.0 <b>Date</b> 25/Nov/2008 <b>Page</b> 26/26
---	---	---

multipole expansion, a Taylor expansion and two weighted interpolation methods. None of them yields satisfactory results. As discussed in the previous sections of this document, the distance weighting interpolation method offers an acceptable average performance for each field component and may be computed with minimum CPU time consumption. A Taylor expansion does not yield better results than the former method, as it occurs as well with the multipole expansion, in spite of being physically sound methods. Additionally, these methods are more computationally expensive.